Numerical investigation into the composite behaviour of over-deformed segmental tunnel linings strengthened by bonding steel plates

Zhai, Wuzhou; Zhang, Dongming; Huang, Hongwei; Chapman, David

DOI:
10.1016/j.sandf.2023.101335

Document Version
Publisher's PDF, also known as Version of record

Citation for published version (Harvard):
Zhai, W, Zhang, D, Huang, H & Chapman, D 2023, 'Numerical investigation into the composite behaviour of over-deformed segmental tunnel linings strengthened by bonding steel plates', *Soils and Foundations*, vol. 63, no. 4, 101335. https://doi.org/10.1016/j.sandf.2023.101335

HOSTED BY
ELSEVIER
Available online at www.sciencedirect.com
ScienceDirect
Soils and Foundations 63 (2023) 101335
SOILS AND FOUNDATIONS
www.elsevier.com/locate/sandf

Technical Paper

Numerical investigation into the composite behaviour of over-deformed segmental tunnel linings strengthened by bonding steel plates ☆

Wuzhou Zhai [a,b], Dongming Zhang [a,*], Hongwei Huang [a], David Chapman [b]

[a] Department of Geotechnical Engineering, College of Civil Engineering, Tongji University, Shanghai, China
[b] National Buried Infrastructure Facility (NBIF), School of Engineering, University of Birmingham, Edgbaston, Birmingham, UK

Received 27 June 2022; received in revised form 11 April 2023; accepted 3 June 2023
Available online 11 July 2023

Abstract

Bonding steel plate has been used as a strengthening approach to repair disrupted segmental lining of operational tunnels. This paper introduces numerical investigation into the composite behaviour of the initially deformed segmental tunnel linings strengthened by bonding steel plates using finite element modelling. Cohesive zone modelling was used to simulate the interface bonding behaviour between the segmental linings and steel plates. The full history of the tunnel behaviour before and after strengthening were simulated, where the segmental tunnel lining is initially loaded to create some deformation, then after bonding steel plate, the strengthened tunnel is reloaded until failure occurs. By comparing the results with experimental data from the literature, the proposed model was proved to be capable of simulating the strengthened lining behaviour and able to capture the strengthening failure process in terms of the interface debonding. Subsequently, the segmental lining response and interface shear stress distribution and propagation were analysed to interpret the interaction and failure mechanism of the steel plate strengthened segmental linings. The influence of the initial deformation and the steel plate thickness were investigated and discussed in terms of the strengthened stiffness and capacity. It has been found that the interface shear stress concentration occurred at the positions of the segment joints, where bond damage first initiated. The ultimate failure of the steel plate strengthening happened suddenly once a local debonding zone close to the segmental joint was formed. In addition, the predicted results indicate that a delay in strengthening would result in an increase in strengthened capacity but a decrease in strengthened stiffness. By using thicker steel plates, the strengthened stiffness was improved, while the strengthened capacity could be improved only if the thickness was relatively thin.

Keywords: Segmetal tunnel linings; Steel plate strengthening; Finite element analysis; Cohesive zone modelling

1. Introduction

Over the past decades, there has been a considerable increase in use of shield-driven tunnels for construction in soft ground areas across the world. The lining systems associated with shield-driven tunnels are commonly made up of precast reinforced concrete segments and bolts, the segmental linings are often designed to behave as the only permanent support system during the service life of the tunnel. However, these long tube-shaped structures buried in soft soils often face risks of being disrupted by close engineering ground works or disturbance, such as adjacent excavations (Chang et al., 2001b), pile drilling (RAIB, 2014), surcharge (Huang et al., 2016), and flooding (Van Empel et al., 2006). In these situations, the segmental linings could possibly be adversely affected if they are not well

Peer review under responsibility of The Japanese Geotechnical Society.
* Corresponding author.
E-mail address: 09zhang@tongji.edu.cn (D. Zhang).

https://doi.org/10.1016/j.sandf.2023.101335
0038-0806/

protected, which threatens the safety of the tunnel operations. Therefore, effective repair measures must be taken to strengthen the degraded or damaged segmental linings so they could be capable of resisting further changes in surrounding loads and environmental conditions. There are several ways to strengthen damage tunnels, amongst these the steel plate strengthening method has been widely adopted due to its advantages, such as strengthening effectiveness and mechanized installation (Kiriyama et al., 2005). This method has been studied and used in many tunnel rehabilitation projects, as shown in Fig. 1. Chang et al. (2001a) introduced a rehabilitation work for deformed segmental tunnel linings due to nearby excavations in Taipei, where steel segments were used to strengthen the damaged tunnel linings. The design and construction procedure were introduced in details. Zhang et al. (2019b) reported a case of over-deformed segmental tunnel linings caused by excessive ground surface surcharge in Shanghai. In this case, epoxy bonded steel plates were used to strengthen the segmental lining rings with horizontal convergence ratios over 2.4%.

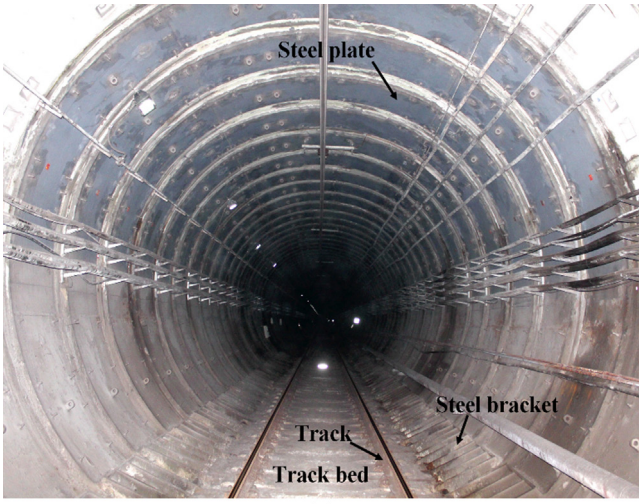

(a)

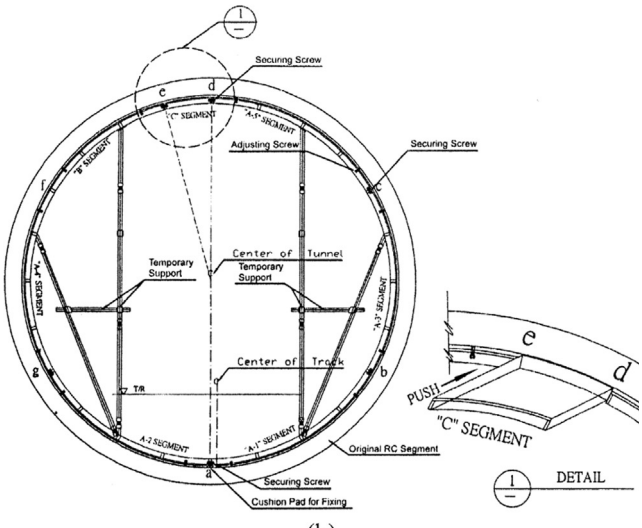

(b)

Fig. 1. Shield-driven tunnels strengthened by steel plates, (a) Shanghai metro tunnels (Zhang et al., 2019b), (b) Taipei transit system tunnel (Chang et al., 2001a).

In order to know how much enhancement to the existing tunnel this steel plate strengthening technique could bring, some researches have been conducted. Taking the Shanghai Metro tunnel as prototypes, both full-scaled (Liu et al., 2017) and small-scaled (Liu et al., 2019; Zhai et al., 2020) laboratory model tests have been performed for strengthening damaged segmental lining rings by bonding steel plates. These experimental works demonstrated the effectiveness of this method and provided valuable data and observations for the composited lining behaviour and strengthening failure process. It is admitted the effectiveness of the plate bonding technique is strongly affected by the performance of the bond interface between the strengthening plate and the concrete substrate, where the strengthening failure happens due to the formation and rapid propagation of interfacial cracks. Although this phenomenon could be observed during the physical experiments, it was currently quite challenging to make precise measurements of the interfacial sliding or strain conditions at the model test scales (Zhang et al., 2019c; Zhai et al., 2020).

Numerical tools offered a good complementary approach, corresponding numerical studies were also performed by researchers using different numerical approaches (Zhao et al., 2016; Zhang et al., 2019a). In all these numerical modelling, the interface between the tunnel linings and the steel plates was simulated using spring elements with nonlinear properties, which was computationally efficient and capable of simulating the composite lining behaviour before strengthening failure occurred. However, such interface modelling approaches like TIE (there is no relative motion between two surfaces with TIE constraints) or spring elements (Zhang et al., 2019a; Li et al., 2021) could not simulate the aforementioned debonding failure in terms of the localized damage initiation and propagation along the interface. An appropriate simulation of interface failure is crucial, it is not only helpful in understanding the interaction mechanism of segmental linings and steel plates, but also useful for predicting the enhanced capacity of the tunnel lining system after strengthening. Therefore, it would be highly demanding for further numerical investigation into the segmental tunnel lining strengthened by steel plates with more precise consideration of the interface bonding behaviour.

The cohesive modelling approach is one of the most efficient techniques in debonding simulations, the concept of which was first proposed by Barenblatt (1959) for crack and fracture problems. It bridges the gap between the stress- and energy-based criteria, and has been widely applied in modelling of fracture under static, dynamic and cycling load conditions (Wang et al., 2019 and 2022). In recent years, the cohesive modelling has been successfully used in debonding analyses for concrete structures

with external bonded plates (Rabinovitch, 2008; De Lorenzis and Zavarise, 2009; Zidani et al., 2015). In terms of cohesive modelling for interfacial bonding problems, the interfacial normal and shear stresses are nonlinearly connected to the normal and tangential relative displacement along the interface. As the bonding interface gradually separates, the bonding stress initially increases to a certain level, then decreases as the separation continues, and finally drops to zero. In this way, the whole debonding process of interface interaction from perfect bonding to complete separation is well captured. With the help of cohesive modelling, the interface stress and displacement conditions could be evaluated to interpret the interaction mechanism between two bonded components.

However, previous study mainly focuses on the ordinary structures like continuous beams or columns, for these types of problems, the initial deformation of the existing structure before strengthening is relatively small and often ignored in previous research. Different from the sample supported beams or columns, the shield tunnel linings are assembled by separate concrete segments with steel bolts, the opening and rotation at these bolt-connected segmental joints results in discontinuous deformation modes of the segmental tunnel linings. As observed in practical cases, the tunnel lining deformation could be relatively large, especially for those tunnels in soft soils. Once the steel plates are bonded to strength the segmental tunnel linings, the complicated interface stress distribution and debonding propagation are certainly affected by these structural discontinuities at the segmental joints. In addition, as an underground structure, the resistance from surrounding soil due to soil-structure interaction accumulates as tunnel deforms (Zhai et al., 2021, 2022). Thus, there is a call for investigation into the influence of deformation degree during the analysis of steel plates strengthening, which could provide fundamental knowledge for determination of rehabilitation timing form a practical point of view.

In this research, a finite element model for segmental tunnel linings strengthened by steel plates was proposed, in which the tunnel-plate interface is simulated using a zero-thickness cohesive zone modelling technique. Validations for the proposed numerical model were conducted with comparison to model test results, which was previously performed and published by the authors. After model validation, the segmental lining behaviour before and after strengthening was analysed by focusing on the joint opening deformation and plastic strain distribution. Then, the bonding stress distribution and propagation along the interface between segmental linings and steel plate was extracted, which provide a thorough investigation into the interaction mechanism and failure process of this tunnel strengthening method. Subsequently, influence of the initial degree of lining deformation and the steel plate thickness have been discussed, to help achieve an optimal design in terms of strengthening timing and materials involved.

2. Finite element modelling

The structural behaviour of segmental tunnel linings strengthened by steel plates was numerically investigated using the finite element package ABAQUS. Details of the model and the modelling process are introduced in this section.

2.1. Finite element mesh and material properties

Assembled by numerous concrete segments with steel bolts, the shield-driven tunnel is initially constructed as a tube-shape with discontinuous joints. The existing of segmental joints make lining stiffness varies unevenly along the tunnel structures, these joints are often the weak chain of the whole support system when the tunnel linings are stressed due to external disturbance (Li et al., 2015). Therefore, the complicated structural behaviour of these segmental joints should be considered appropriately with a consideration of both accuracy and efficiency.

As shown in Fig. 2, a 2D plane strain finite element mesh of the segmental tunnel linings strengthened by steel plates has been established referred to Shanghai metro tunnels. In terms of the lining segments, six precast C50 reinforced concrete segments were assembled to form a ring with an inner radius of 2.7 m and a lining thickness of 0.375 m. The RC segmental lining were modelled by CPE4 elements (4-node plane strain quadrilateral elements) with an elastic-perfectly-plastic property, as shown in

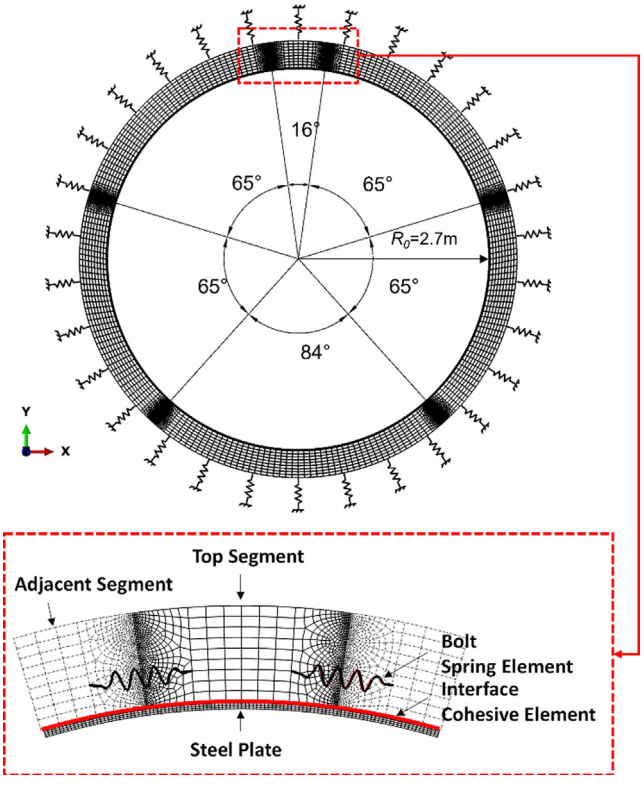

Fig. 2. Finite element mesh of the segmental tunnel linings strengthened by steel plates.

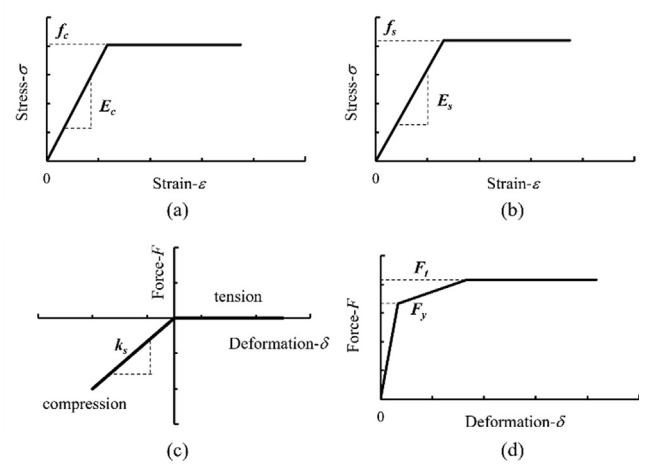

Fig. 3. Constitutive models and material properties, (a) lining concrete, (b) steel, (c) soil springs, (d) segmental joint bolts.

Fig. 3(a). The concrete segments are connected to adjacent ones by straight bolt at the position of the longitudinal joints. The segments were frictionally contacted and connected by straight bolts, which were modelled by the SPRINGA elements with nonlinear properties. The force–deformation relationship for bolt springs is illustrated in Fig. 3 (d), where F_y and F_t are the yield and tensile strength of the bolts.

According to the Guide Lines for the Design of Shield Tunnel Lining proposed by the International Tunnelling Association (ITA, 2000), the lining-soil interaction was considered as the subgrade reaction proportional to the displacement of the ground, which was simulated by a soil spring system as shown in Fig. 2. The soil springs were modelled by SPRING1 elements with a compression-only behaviour as illustrated in Fig. 3 (c). The subgrade reaction coefficient of the soil springs was adopted according to the Shanghai Foundation Design Code (2010).

In terms of the strengthening components, a steel plate was attached to the tunnel internal profile, which was modelled by CPE4 elements with elastic-perfect-plastic steel properties as shown in Fig. 3 (b).

2.2. Concrete-steel bonding interface behaviour

As a composite lining system after strengthening treatment, both shear and normal stresses exist along the steel-tunnel circumferential interface. For simplification purposes in FE analysis, this interface is thought of a very thin layer of adhesive with a constitutive response combining both shear and tension behaviours. Herein, a bilinear traction-separation law for both normal (model-Ⅰ) and tangential (mode-Ⅱ) behaviour was adopted for the cohesive elements. Three characteristic parameters of the bonding interface are captured, i.e., the fracture energy (covered area under the curve), the elastic property (slope of the curve in the elastic stage), and the cohesive strength (peak stress), respectively. In this paper, the mixed mode condition is adopted, which requires suitable criteria for both initiation and propagation of debonding crack. Different interfacial stiffnesses in the elastic stages and cohesive strength are considered for model-Ⅰ and mode-Ⅱ, respectively. The mixed mode bilinear traction-separation law for cohesive modelling is illustrated in Fig. 4, and its fundamental features are summarized in following paragraphs.

The elastic behaviour is determined in terms of the elastic constitutive matrix that relates the nominal stress to nominal strain across the interface as:

$$\begin{bmatrix} t_n \\ t_s \end{bmatrix} = \begin{bmatrix} E_{nn} & E_{ns} \\ E_{ns} & E_{ss} \end{bmatrix} \begin{bmatrix} \varepsilon_n \\ \varepsilon_s \end{bmatrix} \tag{1}$$

where E_{nn} and E_{ss} are compression/tension stiffness and shear stiffness, while E_{ns} is adopted as 0 for uncoupled behaviour (Ziraba and Baluch, 1995). t_n and t_s are nominal normal and shear stresses, and ε_n and ε_s are nominal normal and shear strains, respectively. The nominal stresses are forces components divided by the original area at each integration point, while the nominal strains are the separations divided by the original constitutive thickness at each integration point. The nominal strains are defined as:

$$\varepsilon_n = \delta_n / T_0, \varepsilon_s = \delta_s / T_0 \tag{2}$$

where δ_n and δ_s are corresponding separations, and T_0 is the original constitutive thickness (defaulted as 1.0).

The damage behaviour in the cohesive layer is defined by specifying a damage initiation criterion and a damage evolution law. The damage initiation refers to the beginning of the degradation, while the damage evolution describes the pattern in which cohesive elements are degraded. Once the damage initiation criterion is met, the cohesive layer damage can occur according to the damage evolution law.

The quadratic stress failure criterion is adopted for the damage initiation of the cohesive elements. It is assumed that the onset of softening occurs when equation (3) is fulfilled.

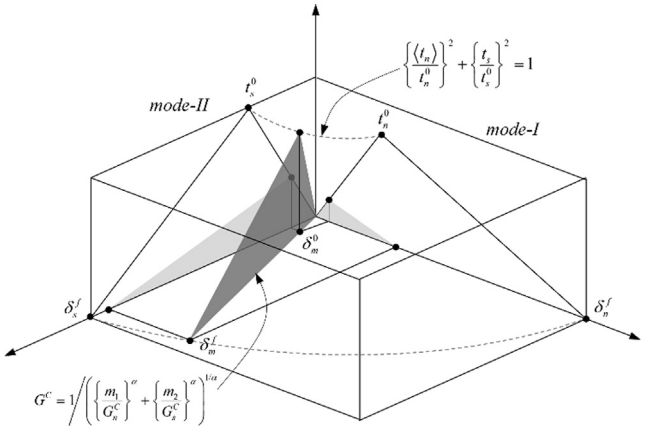

Fig. 4. Mixed mode traction-separation law for the cohesive modelling (Camanho and Dávila, 2002; Systemes, 2017).

$$\left(\frac{\langle t_n \rangle}{t_n^0}\right)^2 + \left(\frac{t_s}{t_s^0}\right)^2 = 1 \tag{3}$$

where t_n^0 and t_s^0 represent peak values of nominal stress, Macaulay operator $\langle\rangle$ implies that the negative normal stress (compression) is assumed not to initiate damage.

The damage evolution law describes the rate at which the cohesive material stiffness is degraded once the damage initiation criterion is reached. The stress components of the traction-separation model are developed due to damage according to:

$$\begin{aligned} t_n &= \begin{cases} (1-D)\,\bar{t}_n, \bar{t}_n \geqslant 0 \\ \bar{t}_n, \bar{t}_n < 0 \end{cases} \\ t_s &= (1-D)\,t_s^- \end{aligned} \tag{4}$$

where $\bar{t}_n$ and $\bar{t}_s$ are stress components predicted by the elastic traction-separation behaviour for the current strains without damage, and d is the damage variable. The linear damage evolution law based on energy is adopted in this paper, according to which the damage variable D is evaluated as:

$$D = \frac{\delta_m^f\left(\delta_m^{\max} - \delta_m^0\right)}{\delta_m^{\max}\left(\delta_m^f - \delta_m^0\right)} \tag{5}$$

$$\delta_m = \sqrt{\langle \delta_n \rangle^2 + \delta_s^2},\ \delta_m^f = 2G_c/t_{eff}^0 \tag{6}$$

where δ_m is the effective displacement, which is introduced to describe the damage evolution under a combination of normal and shear deformation. δ_m^f is the effective displacement at complete failure, δ_m^0 is the effective displacement at the damage initiation, δ_m^{max} is the maximum effective displacement during the loading history, G_c is the energy dissipating due to failure, t_{eff}^0 is the effective traction at the damage initiation.

In Abaqus 2017, a library of cohesive elements is offered to model the behavior of adhesive bonding interfaces. In this work, the implementation of cohesive modelling was conducted in Abaqus/Standard CAE environment following the Abaqus User's Manual (Systemes, 2017). All essential parameters that need to be given are presented in Table 1. In terms of the elastic parameters, elastic stiffness values are referred to the research on reinforced concrete strengthened by epoxy-bonded steel plates conducted by Jones et al. (1988), which were also used and validated in the numerical work performed by Adhikary and Mutsuyoshi (2002). In terms of the damage parameters, peak stress and fracture energy are determined according to study on concrete with external bonded plates performed by Lu et al. (2005), which were used and validated in the numerical work on strengthening RC beams with bonding plates conducted by Zidani et al. (2015).

Table 1
Parameters of the traction-separation model for the interfacial cohesive elements.

	Parameters	Symbol	Unit	Value
Cohesive element properties	Normal stiffness	E_{nn}	*MPa/mm*	144
	Shear stiffness	E_{ss}	*MPa/mm*	60
	Peak nominal norm stress	t_n^0	*MPa*	9
	Peak nominal shear stress	t_s^0	*MPa*	4.5
	Interface fracture energy	G_c	*N/mm*	0.4

2.3. Loads and modelling procedures

According to the shield tunnel lining design guidelines proposed by ITA (2000), a schematic of the load conditions for the shallow buried circular tunnel is shown in Fig. 5. The vertical earth pressure at the tunnel crown $q_1 = (H - R_H cos\theta)\gamma_s$, the vertical earth pressure at tunnel invert $q_2 = (H - \pi/4R_H)\gamma_s$, the lateral earth pressure $e = k_0(H - R_H cos\theta)\gamma_s$ and the surcharge load (q_s) are considered in this study. H is tunnel depth, R_H is radius of lining centroid, γ_s is the unit weight of soils and k_0 is the earth pressure coefficient.

In order to capture the whole history of structural response of segmental tunnel linings before and after the steel plate strengthening, the simulation is conducted in sequence of several steps. The modelling procedure is demonstrated in terms of the relationship between the surcharge load and the corresponding tunnel deformation, as illustrated in Fig. 6. In this figure, δ_0 and P_0 indicate the existing tunnel deformation and surcharge load level when the steel plate strengthening is implemented, namely the "Strengthening Point". δ_u and P_u indicate the tunnel deformation and surcharge load level when the segmental lining strengthened by steel plate reach its capacity, namely the "Strengthening Failure Point". It is noted that, in the rehabilitation practice of deformed segmental tunnel linings, the existing deformation is often measured as a general indicator to evaluate the tunnel lining performance, which

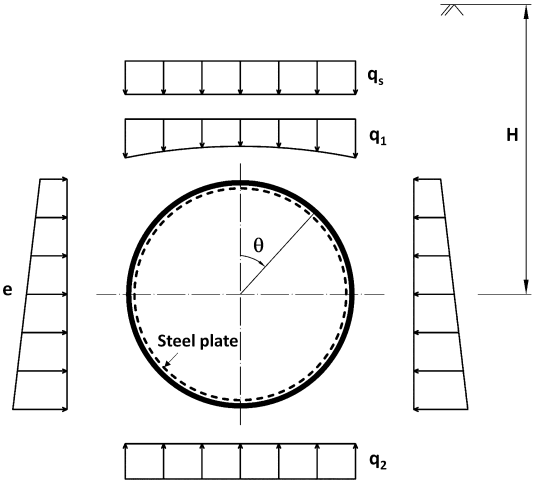

Fig. 5. A schematic of the load conditions.

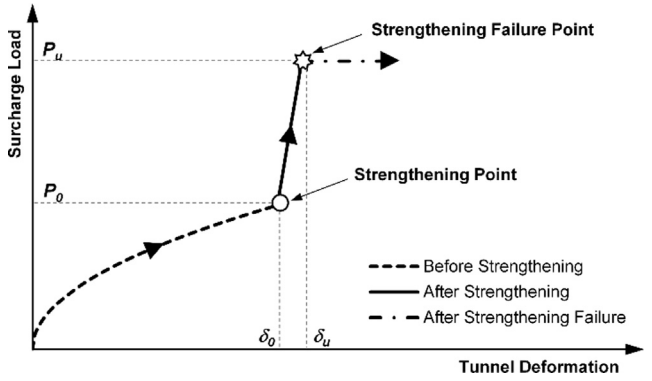

Fig. 6. Illustration of the modelling procedures in terms of the tunnel load-deformation relationship.

is the key reference for the determination of the timing of strengthening implementation. Therefore, the value of δ_0 is used to indicate the timing of strengthening in this paper, where a smaller δ_0 implies earlier implementation of the steel plate strengthening. In addition, the value of P_u is used to indicate the capacity of strengthened tunnel linings, where a larger P_u implies higher lining capacity after the implementation of steel plate strengthening.

Initially, the earth pressure loads were applied to the tunnel without the steel plate strengthening (steel plates elements were deactivated). Subsequently, the surcharge load was applied, and the tunnel lining deformed as the load increased. Once the tunnel lining deformed to a certain level, namely the strengthening point, the steel plate elements were activated to achieve the simulation of strengthening deformed segmental tunnel linings. Then, the surcharge load continued to be increased on the strengthened tunnel until the strengthening failure occurred, after which the surcharged load could not be increased further. This whole process is presented as a load-deformation curve with three phases shown in Fig. 6.

3. Comparisons between the simulation and test results

Zhai et al. (2020) performed a laboratory model test for strengthening damaged segmental tunnel lining using steel plates. This experiment was designed by scaling from the actual segmental linings with an outer diameter of 6.2 m of the Shanghai Metro tunnel. For comparison purposes, the geometry and material parameters for the proposed numerical model were determined according to the experimental prototype, as given in Fig. 2 and Table 2. In this experimental study, the rubber particles were utilized to simulate deformational properties of layer No.③ to ⑤ clay soil in Shanghai, where local metro tunnels were usually constructed. According to the Shanghai Foundation Design Code DGJ08-11–2010, a subgrade reaction coefficient of 3000 kN/m^3 is recommended for this type of soils. Therefore, in order to simulate compression only soil-tunnel interactions, the compressive stiffness was evaluated by multiplying the subgrade reaction coefficient by element dimension on the tunnel extrados, while the tensile stiffness was adopted as 0.

The results from test No.2 of the experimental study (Zhai et al., 2020) were selected, in which the segmental tunnel linings were first deformed to a certain level ($\frac{\Delta D_h}{D} = 2.2\%$), and then loaded until strengthening failure occurred. The same process was simulated by the FE model proposed in this paper, and the results from the experiment and simulation were compared in terms of the lining displacement, the steel plate stains, and the segmental joint responses.

3.1. Lining deformation

As shown in Fig. 7, the horizontal diameter changes of the segmental tunnel linings due to increasing surcharge load were compared between the numerical simulation results and the model test measurements. The deformation and surcharge values are normalized as dimensionless values, namely $\Delta D_h/D$ and $q_s/\gamma h$, for the × and y axis. It had been observed in the model test: before the steel plate strengthening, the segmental tunnel lining deformed nonlinearly as rotation occurred at the joints between adjacent segments; after the steel plate strengthening, the lining stiffness was improved significantly; as the surcharge load increased, the strengthened lining stiffness suddenly van-

Table 2
Material properties of the numerical simulation.

	Properties	Symbol	Unit	Value
Reinforced concrete of segmental linings	Compressive strength	f_c	MPa	32.4
	Poisson's ratio	ν_c	–	0.28
	Elastic modulus	E_c	MPa	34.5
Steel plates	Elastic modulus	E_s	MPa	200
	Poisson's ratio	ν_s	–	0.2
	Thickness	t_s	mm	30
Joint bolts	Grade	–	–	5.8
	Diameter	d	mm	30
	Length	l	mm	400
Soils	Subgrade reaction coefficient(compression)	k_s^-	kN/m^3	3000
	Subgrade reaction coefficient(tension)	k_s^+	kN/m^3	0
	Unit weight	γ	kN/m^3	16
	Lateral pressure coefficient	k_0	–	0.45

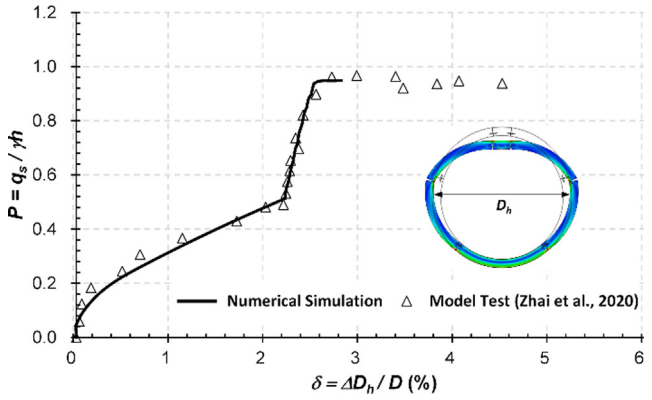

Fig. 7. Comparison of the numerical and experimental results in terms of the tunnel lining deformation.

ished once debonding failure occurred at the interface. This whole process is characterized in terms of a load-deformation relationship, which is represented by the triangular symbols in Fig. 7. This process was simulated numerically using the proposed FE model, which is represented by a load-deformation curve in this figure. Three phases, namely before strengthening, after strengthening and strengthening failure, were all simulated. As seen in Fig. 7, there is a good agreement between the numerical simulation results and the model test data in terms of lining displacements.

3.2. Steel plate strains

In the model test, once the strengthening procedure was completed, strain gauges were attached to the plate so that strains in the circumferential direction could be measured. Therefore, the corresponding strains within the steel plates were extracted from the numerical simulation results for comparison purposes. Fig. 8 (a) shows the steel plate strains at the location of the tunnel crown, where the measured tensile strains (positive) demonstrated that the steel plates were in tension at this location. Fig. 8 (b) shows the steel plate strains at the location of the tunnel spring line, where the measured compressive strains (negative) demonstrated that the steel plates were in compression at this location. In both figures, the plate strain magnitudes continued increasing as the surcharge load increased, until an interface debonding failure occurred. A significant drop in the steel plate strains was observed just after the strengthening failure occurrence.

In both two figures, good agreements in trends were observed between the simulated strain values and the test measurements. Gaps between two curves became larger when the strengthened tunnel was stressed towards failure. In the experiment, the tunnel lining was modelled by gypsum, where cracks propagated within linings. While the segmental linings were simulated as continuum in finite element modelling. Comparing with the uncracked linings, the opening of cracks would relive strains in adjacent material.

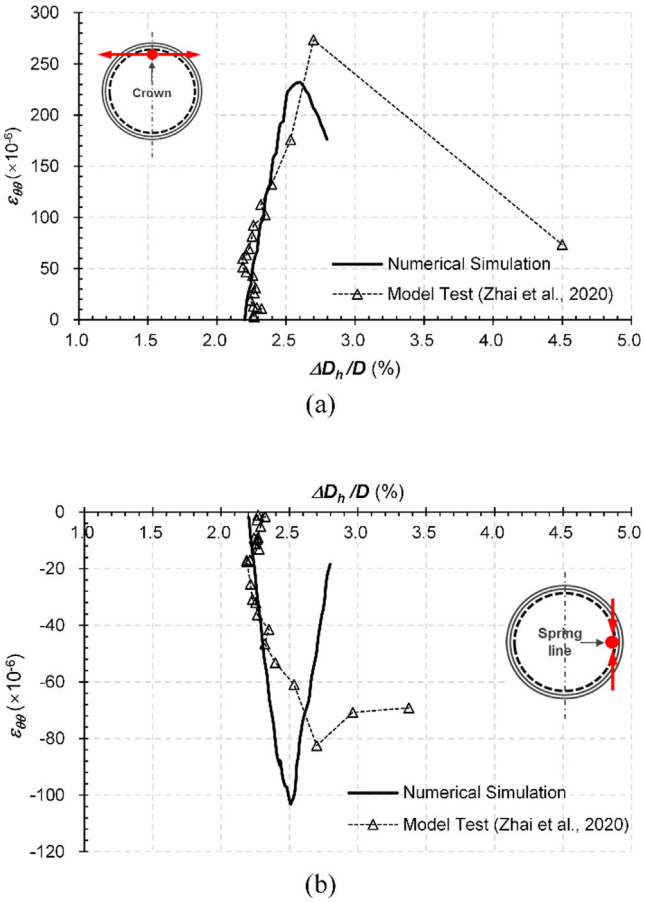

Fig. 8. Comparison of steel plate strains between the numerical and the experimental resultsJoint behaviour, (a) steel plate strains at the tunnel crown, (b) steel plate strains at the tunnel spring line.

Therefore, as shown in Fig. 8, strains from numerical simulation were larger than those from the model test.

Joints are the critical parts which influence segmental tunnel lining behaviour (Gong et al., 2017 and 2023), the simulated joint responses were extracted and compared to those observations from the model test. Changes in the joint opening as the surcharge load increased were shown in Fig. 9. The × axis represents the relative surcharge level calculated by P/P_u, where P is the surcharge and P_u is the maximum surcharge when strengthening failure happened. Before the strengthening point, the joint opening value at different tunnel positions all increased with rising gradients, which indicated a gradual reduction in the joint rotation stiffness. After the strengthened point, the opening trend of all the joints were significantly restricted. There were little changes in the opening values of joints #2 and #3 as the surcharge increased, while abrupt rises were observed when strengthening failure suddenly occurred. The opening value of joint at the tunnel crown was larger than those of the joints at the other two positions.

In order to explain the reason for the observed trends of the joint opening, the concrete and bolt behaviour at segmental joints at different locations were analysed. Fig. 10 shows the responses of joint close to tunnel crown (joint

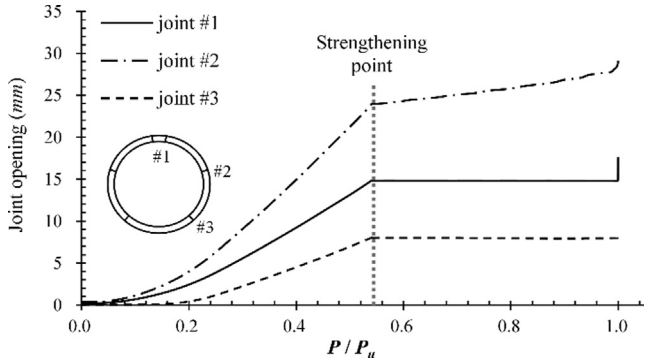

Fig. 9. Changes in the opening of joints at different tunnel lining positions.

#1). As shown in Fig. 10 (a), segmental linings were rotated with opening at intrados, the extrados concrete was compressed into plasticity, and bolt sustained tension. It is seen that the simulated joint rotating deformation pattern shows a good agreement with that observation in the model test as shown in Fig. 10 (b). The accumulated concrete plastic strain and bolt strain at joint #1 were shown in Fig. 10 (c) and (d) respectively. Before the steel plate strengthening was implemented, both the concrete plastic compressive strain and the bolt tensile strain increased rapidly. After the steel plate strengthening, increase in both the concrete plastic strain and the bolt strain were restricted and kept stable.

Fig. 11 presents structural response of the segmental joint close to tunnel spring line. As shown in Fig. 11 (a), segmental linings were rotated with opening at extrados, the intrados concrete was compressed into plasticity. In the model test, extrados opening and intrados concrete crash were observed as shown in Fig. 11 (b), which provides a good validation to the simulation results in terms of joint deformation patterns. The accumulated concrete plastic strain and bolt strain at joint #2 were shown in Fig. 11 (c) and (d) respectively. It is seen that the concrete and bolt strain increased rapidly until the steel plate strengthening was implemented.

Based on above comparisons between the simulation and model test results, it is confident to say that the proposed FE modelling has shown capabilities of simulating the whole process of strengthening deformed segmental tunnel linings by bonding steel plates, and to predicate the structural behaviour of composited linings accurately in the post-strengthening stage.

4. Results and discussion

4.1. Segmental tunnel lining behaviour

Fig. 12 shows the stress distribution in the segmental tunnel lining strengthened by steel plates in terms of Mises stress. It is observed that the segmental tunnel lining and the steel plate behaved as a composite lining system after strengthening. Stress condition in the steel plate varied at different positions, where significant stress concentration was observed within the area close to locations of the segmental joints. In order to understand the steel plate behaviour, the steel stress at positions of joints #1 and #2 were extracted as shown in Fig. 13. Fig. 13 (a) presents the steel plate stress at joint #1 near the tunnel crown, where the steel plate was stressed on the opening side of the segment joint. The tensile stress increased rapidly until a sudden drop occurred when the strengthening failure happened. The maximum tensile stress was 49.9 MPa. Fig. 13 (b) presents the steel plate stress at joint #2 near the tunnel spring line, where the steel plate was stressed on the compressed side of the segment joint. The compres-

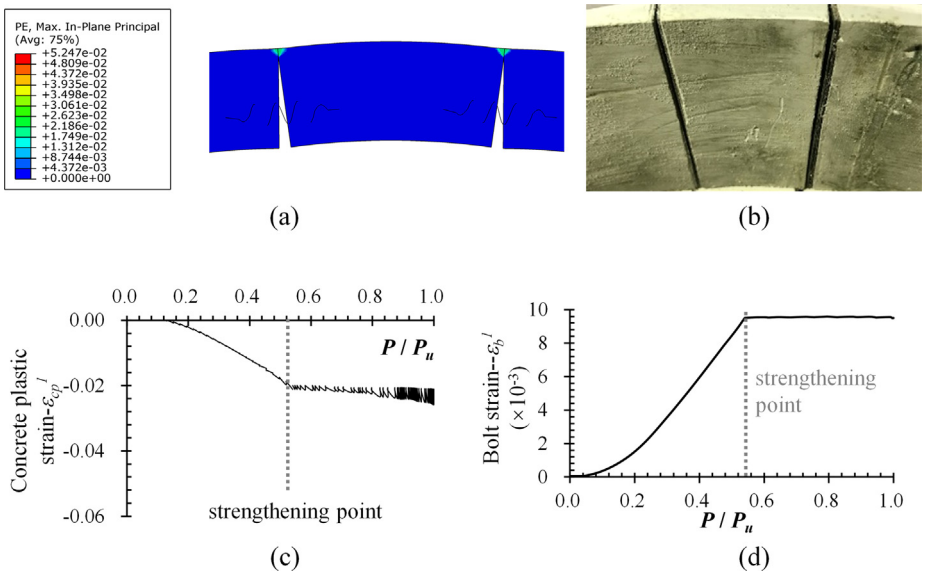

Fig. 10. Structural response of the joint #1, (a) simulated joint deformation and plastic strain accumulation, (b) joint opening in model test, (c) concrete plastic strain, (d) bolt strain.

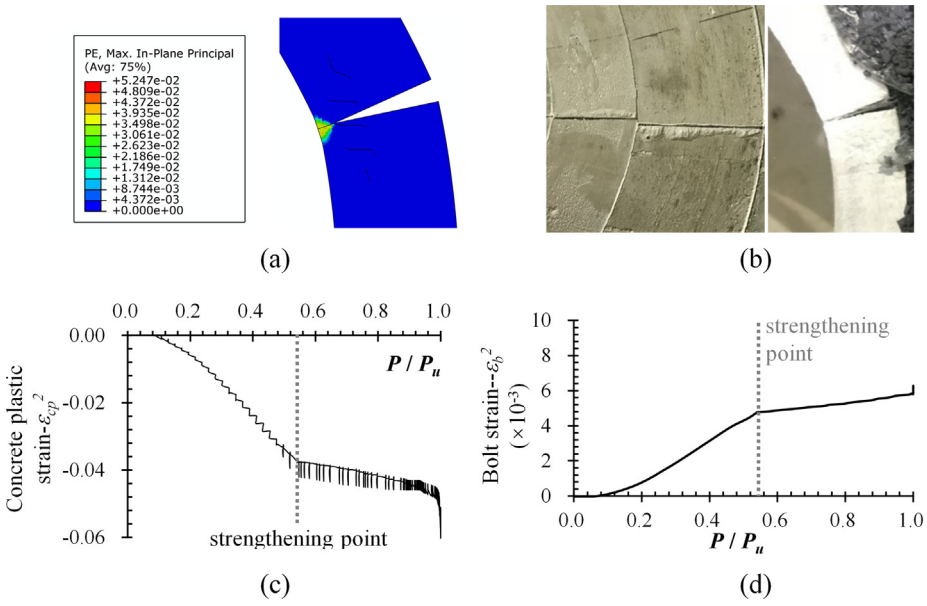

Fig. 11. Structural response of the joint #2, (a) simulated joint deformation and plastic strain accumulation, (b) joint opening in model test, (c) concrete plastic strain, (d) bolt strain.

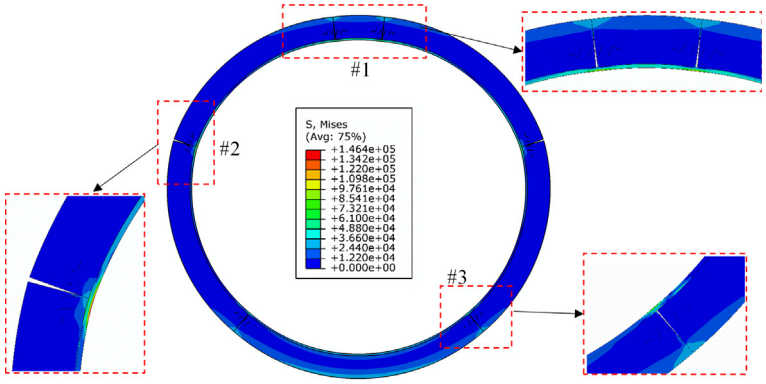

Fig. 12. Stress contour of the segmental tunnel lining strengthened by steel plates.

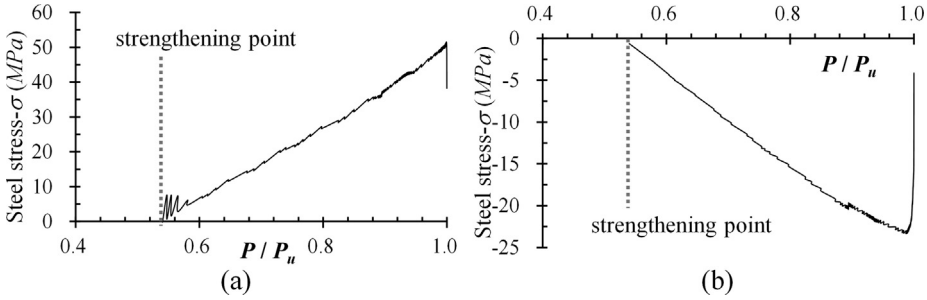

Fig. 13. Stress in the steel plate at different tunnel positions, (a) joint #1, (b) joint #2.

sive stress increased rapidly until a sudden drop occurred when the strengthening failure happened. The maximum compressive stress was 23.3 MPa. The stiffness of segmental joint was improved due to contribution from the steel plate.

4.2. Interface shear stress

Interface is always the critical part for RC structures strengthened by external bonding plates. For tunnel strengthening problems, a well-bonded interface is a guar-

antee of the interaction between the original segmental lining and the steel plate. This very interaction makes the two components behave compatibly as a composite lining support system. In addition, the capacity of the strengthened lining system is also determined by the interface properties. The strengthening failure will occur once the interface stresses exceed the interfacial layer strength. Therefore, a thorough understanding of the stress distribution and the evolution along the interface is essential for both mechanism interpretation and capacity prediction of this steel plates strengthening technique for deformed segmental tunnel linings.

As presented in Fig. 14 and Fig. 15, the distribution and evolution of the shear stresses at the interface between the segmental tunnel lining and the steel plate are extracted from the simulation results. This helps us understand the tunnel-plate interaction mechanism and the strengthening failure process in terms of interface debonding. As shown in Fig. 14, the orientation of the interface shear stress varied circumferentially due to the existence of the segmental joints.

As shown in Fig. 15, the interface shear stresses are displayed at different surcharge load levels, namely 68%, 87%, 99% and 100% P_u, where is P_u is the capacity of the strengthened lining predicted using the FE model (as seen in Fig. 7).

It is observed that shear stress concentration occurred at the positions of the segment joints, while the stress ratio stayed relatively low at other positions, as shown in Fig. 15 (a). This is due to the existence of structural discontinuity between the adjacent segments at positions of the joints. As the strengthened lining continued to deform ovally, the adjacent segments trended to rotate against each other at the joint positions. The joint at $\theta_{j-1} = 8^{\circ}$ (between segment S-1 and S-2) trended to open inward, while the joint at $\theta_{j-2} = 73^{\circ}$ (between segment S-2 and S-3) trended to open outward. The existence of the steel plate behaved against this trend of deformation through the shear force along the interface. Therefore, the stress orientation changes were observed at the positions of these two joints. The maximum shear stress appeared at a position very close to the joint between S-2 and S-3. The entire shear stresses increased as the load increased.

The peak shear stress first hit the bonding strength of the adhesive interface when $P = 87\%\ P_u$, as shown in Fig. 15 (b). Then, the peak stress point moved toward the direction of the tunnel crown along the interface, and the area from the peak stress point to the joint at

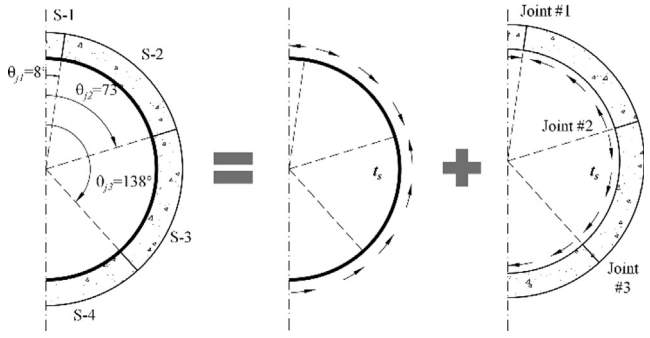

Fig. 14. A schematic of the shear stresses between the segmental lining and the steel plate.

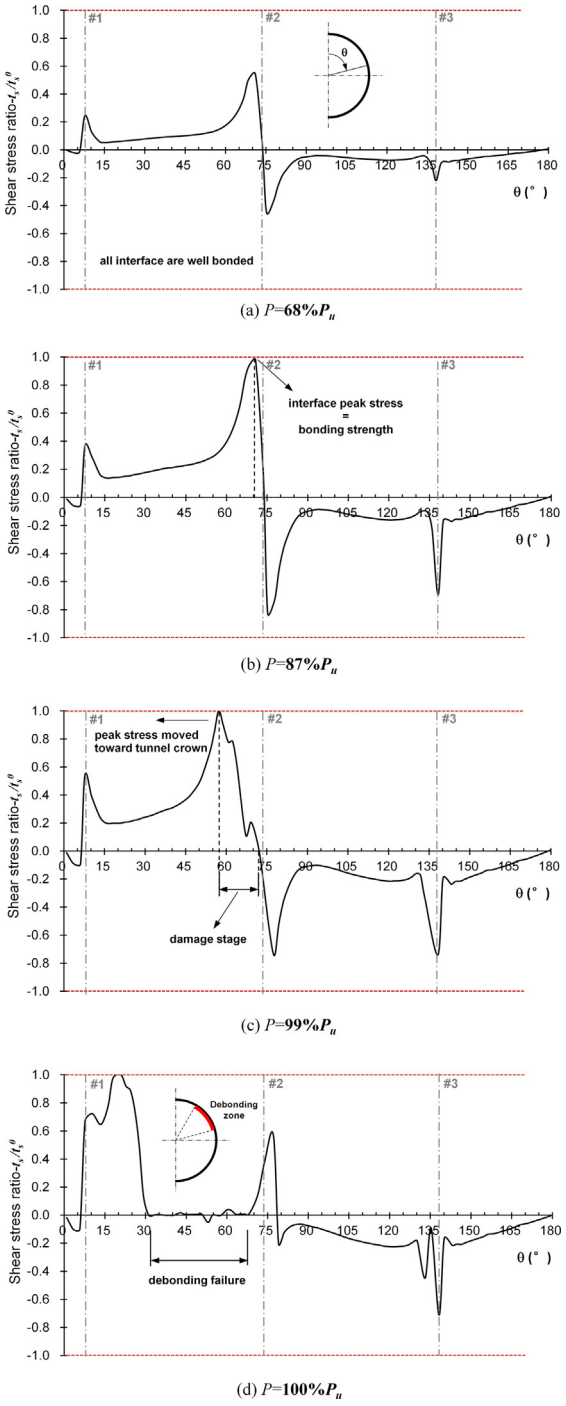

Fig. 15. Distribution of the interface shear stress of the segmental lining strengthened by steel plates at different load levels, (a) P = 68%P_u, (b) P = 87%P_u, (c) P = 99%P_u, (d) P = 100%P_u. (Coordinates of joint #1 #2 and #3 are indicated by grey dashed lines).

$\theta_{j-2} = 73^{\circ}$ started to damage, as shown in Fig. 15 (c). This area propagated and expanded toward the tunnel crown very rapidly. When $P = 100\%\ P_u$, the area from $\theta = 32^{\circ} to 67^{\circ}$ had debonded, while the cohesive elements within the rest of the interface area was not yet damaged. However, the steel plates strengthening had totally failed.

4.3. Influence of the tunnel initial degree of deformation

In practical works of strengthening deformed tunnels using steel plates, there is always a question about when the strengthening should take place, in other words, when is the optimal time to apply the strengthening. The timing of the strengthening is vital because a premature strengthening would cause extra cost, while a delayed strengthening would worsen the risk of operational safety of the tunnel. Therefore, it is important to understand the influence of the strengthening timing.

Using the developed FE model, segmental tunnel linings strengthened at different initial damaged degrees were simulated and presented in terms of P-δ relations as shown in Fig. 16. It is observed that as the initial lining deformation before the strengthening increased, the slope of the strengthened curved decreased and the maximum surcharge at the failure point increased. This means that a delay in strengthening would lead to an increase in capacity but a decrease in stiffness of the strengthening tunnel linings. For comparison purposes, the strengthened stiffness (K) is defined as the curve slope and the strengthened capacity (P_u) are defined as the surcharge load at the strengthening failure point. The trends of these two indexes are shown in Fig. 17.

As shown in Fig. 17, as the initial tunnel deformation before strengthening changed from 1.0% to 6.4%, the strengthened lining stiffness decreased by 45.5%, while the strengthened lining capacity increased by 35.2%. The reason is that as the initial deformation before strengthening increases, more capacity of the original segmental lining is utilized, and its structural condition gets worse due to the segment damage and joint opening. After strengthening, the lining performance is improved on the base of

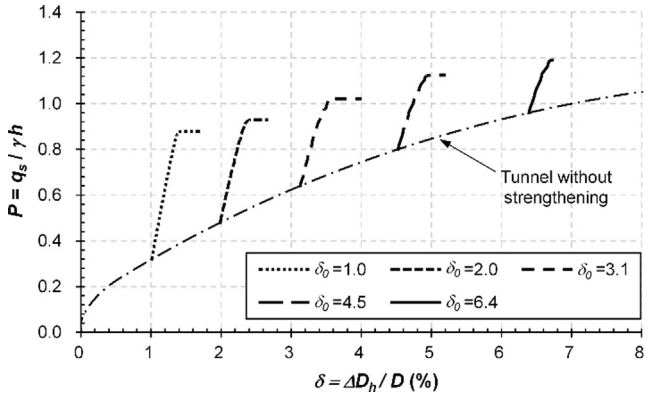

Fig. 16. Performances of segmental tunnel linings strengthened at different initial degrees of deformation.

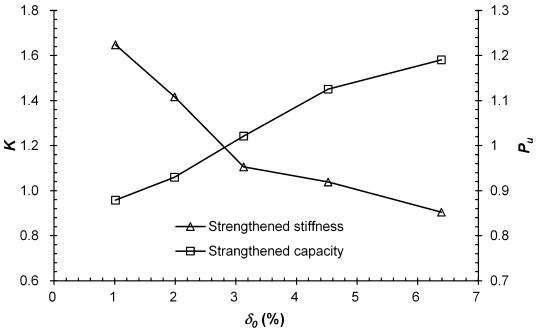

Fig. 17. Influence of the initial degree of deformation on the stiffness and the capacity of the strengthened segmental tunnel linings.

the lining condition before strengthening. Thus, a decrease in stiffness and an increase in capacity of the strengthened lining is observed.

In addition, delay in strengthening means more tunnel deformation would be allowed to happen. When the tunnel is strengthened in an early stage, it benefits in deformation control and strengthened tunnel stiffness, but it results in a lower capacity and higher cost in practice since more rings should be strengthened. When the tunnel is strengthened quite late, it benefits in the strengthened tunnel capacity and lower cost in practice since less rings would be strengthened, but it results in larger deformation and lower stiffness of the tunnel lining after strengthening. Eventually, it comes to a trade-off issue, which is about balancing between the advantages and disadvantages in terms of stiffness, capacity, and total cost.

4.4. Influence of the steel plate thickness

The steel plate thickness is the most critical parameter of a design for strengthening existing tunnels. From an engineering point of view, a thicker plate would possibly provide a stronger support. However, the increase in strengthening materials would also bring difficulties in construction and increased cost. Therefore, it is important to investigate the influences of the steel plate thickness on the strengthening effectiveness of the segmental tunnel lining.

Using the developed FE model, tunnels with the same initial degree of damage were strengthened by steel plates with different thicknesses (5 mm to 30 mm with an interval of 5 mm), their performance are shown in Fig. 18 in terms of a P-δ relationship. It is observed that as the steel plate thickness increased, the stiffness of the strengthened tunnel was improved, while the capacity increased until a certain level. For comparison purposes, the strengthened stiffness and the capacity indexes were evaluated for different steel plate thicknesses.

As shown in Fig. 19, as the steel plate thickness increased from 5 mm to 30 mm, the strengthened stiffness increased by 78.9% with a relatively linear relationship, while the strengthened capacity first increased from 0.82 to 0.94 as the steel plate thickness increased from 5 mm

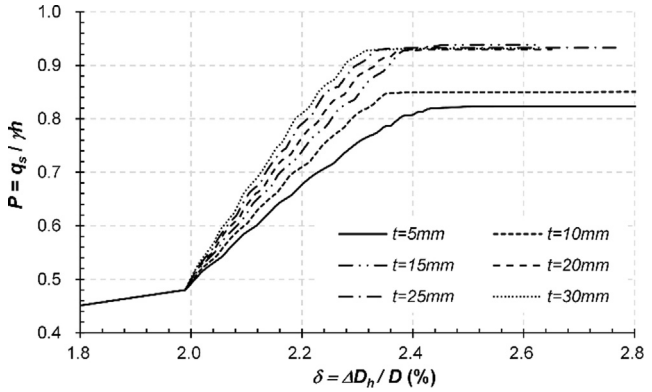

Fig. 18. Performances of segmental tunnel linings strengthened by steel plates with different plate thickness values.

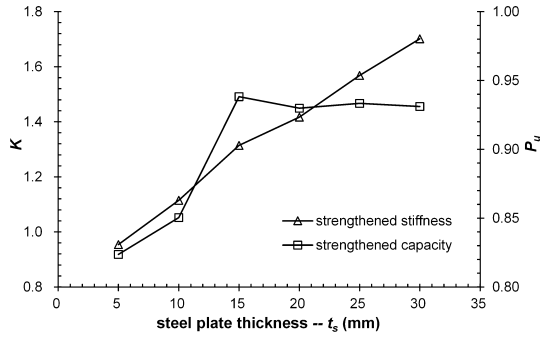

Fig. 19. Influence of the steel plate thickness on the stiffness and the capacity of segmental tunnel linings.

to 15 mm, and then stayed around 0.93 despite the thickening of the plates. The reason is that the thickening of the steel plates could improve the capacity of the strengthened lining when the plate thickness was relative thin (less than 15 mm in this case). However, as the steel plates became relative thick (over 15 mm in this case), the thickening of steel plate could no longer enhance the capacity of the strengthened tunnel, since it was mainly determined by the interface property.

5. Conclusion

In this paper, the composite structural behaviour of segmental tunnel linings strengthened by steel plates was investigated using finite element approaches. The bonding behaviour of the tunnel-plate interface were simulated using cohesive elements with a traction-separation constitutive behaviour. The numerical simulation result was carefully validated by comparison with experiment data. Using this model, the influences of the initial damage degree before strengthening and the steel plate thickness were analysed. Some conclusions could be draw from this study as follows:

(1) The structural stiffness of segmental lining is degraded gradually as the tunnel deforms from a circle to an elliptical shape due to surcharge loads. By strengthening the deformed segmental tunnel lining using steel plates, the deterioration of the lining plasticity at the segment joint are well controlled, and both the structural stiffness and the capacity of the segmental tunnel linings are improved significantly.

(2) There is a significant variation in the shear stress conditions along the tunnel-plate interface. The interface shear stress concentrates at areas close to the segmental joints. The maximum shear stress is located at the joint near the tunnel spring line (between segments S-2 and S-3). Once the maximum shear stress reaches the bonding strength, a debonded area arises and starts to propagate very rapidly. This results in a final failure of the entire steel plate strengthening, when the debonded area are formed within the circumference area from $\theta = 32°$ to $67°$ along the interface between the segmental linings and steel plates.

(3) The effect of the steel plate strengthening is influenced by the initial degree of damage of the tunnel lining before strengthening. A delay in strengthening timing will cause a decrease in stiffness and an increase in the capacity of the segmental tunnel lining strengthened by the steel plates. In the case analysed in this paper, as the initial tunnel deformation before strengthening changed from 1.0% to 6.4%, the strengthened lining stiffness decreased by 45.5%, while the strengthened lining capacity increased by 35.2%.

(4) A thicker steel plate can make the strengthened lining stiffer only if the steel plate is relatively thin. In terms of the case discussed in this paper, the strengthened capacity can be improved by increasing the steel plate thickness, only when the thickness is less than 15 mm. When steel plates over 15 mm are used, the strengthened capacity will not improve by increasing plate thickness.

Additionally, this paper mainly focused on the composite behavior of segmental tunnel lining strengthened by steel plates with emphasis on the interface bonding performance. In real-world applications of steel plate strengthening for tunnels, anchor bolts could be used for higher connection between tunnel linings and steel plates, and the steel plate would not be able to be bonded to the whole range of tunnel ring intrados due to the existing of rail tracks. More investigation should be conducted to further understand the influence of these configurations.

Declaration of Competing Interest

The authors declare that they have no known competing financial interests or personal relationships that could have appeared to influence the work reported in this paper.

Acknowledgement

This study is substantially supported by the National Natural Science Foundation of China (grant No.52130805 and No.52022070), and Shanghai Technology Standard Projects for the Technological Innovation (No. 22DZ2206200). The authors would like to show their great appreciation.

References

Adhikary, B.B., Mutsuyoshi, H., 2002. Numerical simulation of steel-plate strengthened concrete beam by a non-linear finite element method model. Constr. Build. Mater. 16, 291–301.

Barenblatt, G.I., 1959. The formation of equilibrium cracks during brittle fracture. General ideas and hypotheses. Axially-symmetric cracks. J. Appl. Math. Mech. 23, 622–636.

Camanho, P.P. and Dávila, C.G., 2002. Mixed-mode decohesion finite elements for the simulation of delamination in composite materials, NASA/TM-2002–211737, pp. 1–37, 2002.

Chang, C.T., Wang, M.J., Chang, C.T., Sun, C.W., 2001a. Repair of displaced shield tunnel of the Taipei rapid transit system. Tunn. Undergr. Space Technol. 16, 167–173.

Chang, C.T., Sun, C.W., Duann, S.W., Hwang, R.N., 2001b. Response of a Taipei Rapid Transit System (TRTS) tunnel to adjacent excavation. Tunn. Undergr. Space Technol. 16, 151–158.

De Lorenzis, L., Zavarise, G., 2009. Cohesive zone modeling of interfacial stresses in plated beams. Int. J. Solids Struct. 46, 4181–4191.

Gong, C., Ding, W., Mosalam, K.M., Günay, S., Soga, K., 2017. Comparison of the structural behavior of reinforced concrete and steel fiber reinforced concrete tunnel segmental joints. Tunn. Undergr. Space Technol. 68, 38–57.

Gong, C., Kang, L., Liu, L., Lei, M., Ding, W., Yang, Z., 2023. A novel prediction model of packing density for single and hybrid steel fiber-aggregate mixtures. Powder Technol. 418 118295.

Huang, H., Shao, H., Zhang, D., Wang, F., 2016. Deformational responses of operated shield tunnel to extreme surcharge: a case study. Struct. Infrastruct. Eng. 13, 345–360.

ITA (International Tunneling and Underground Space Association), 2000. Guidelines for the design of shield tunnel lining. *Tunnelling and Underground Space Technology,* 15**,** 303-331.

Jones, R., Swamy, R., Charif, A., 1988. Plate separation and anchorage of reinforced concrete beams strengthened by epoxy-bonded steel plates. Struct. Eng. 66.

Kiriyama, K., Kakizaki, M., Takabayashi, T., Hirosawa, N., Takeuchi, T., Hajohta, H., Yano, Y., Imafuku, K., 2005. Structure and construction examples of tunnel reinforcement method using thin steel panels. Nippon Steel Tech. Rep. 92, 45–50.

Li, X., Yan, Z., Wang, Z., Zhu, H., 2015. A progressive model to simulate the full mechanical behavior of concrete segmental lining longitudinal joints. Eng. Struct. 93, 97–113.

Li, X., Zhang, T., Ding, Z., Yang, X., Wen, J., 2021. Numerical analysis of normal concrete lining strengthening methods under different damage levels. Struct. Infrastruct. Eng. 17, 1597–1611.

Liu, X., Jiang, Z., Yuan, Y., Mang, H.A., 2017. Experimental investigation of the ultimate bearing capacity of deformed segmental tunnel linings strengthened by epoxy-bonded steel plates. Struct. Infrastruct. Eng. 14, 685–700.

Liu, X., Lai, H., Sang, Y., 2019. Case study on the model test of staggered-jointed assembling shield tunnel structure reinforced by bonded steel plates under large deformation. IOP Conf. Ser.: Earth Environ. Sci. 330 022080.

Lu, X., Teng, J., Ye, L., Jiang, J., 2005. Bond–slip models for FRP sheets/plates bonded to concrete. Eng. Struct. 27, 920–937.

Rabinovitch, O., 2008. Debonding analysis of fiber-reinforced-polymer strengthened beams: Cohesive zone modeling versus a linear elastic fracture mechanics approach. Eng. Fract. Mech. 75, 2842–2859.

RAIB 2014. Rail Accident Report: Penetration and obstruction of a tunnel between Old Street and Essex Road stations, London 8 March 2013. Derby, UK: Rail Accident Investigation Branch, Department for Transport.

Systemes, D., 2017. SIMULIA user assistance 2017. Dassault Systèmes, Providence, RI.

Van Empel, W., Sip, J., Haring, F., 2006. Design of repair measures of a damaged shield driven tunnel. Tunn. Undergr. Space Technol. 21.

Wang, F., Zhou, M., Zhang, D., Huang, H., Chapman, D., 2019. Random evolution of multiple cracks and associated mechanical behaviors of segmental tunnel linings using a multiscale modeling method. Tunn. Undergr. Space Technol. 90, 220–230.

Wang, F., Ding, C., Pan, H., Zhang, S., 2022. A mesostructure-informed cohesion-based numerical method for fracture behavior of slate with foliation structure. Int. J. Rock Mech. Min. Sci. 160 105252.

Zhai, W., Chapman, D., Zhang, D., Huang, H., 2020. Experimental study on the effectiveness of strengthening over-deformed segmental tunnel lining by steel plates. Tunn. Undergr. Space Technol. 104 103530.

Zhai, W., Chapman, D., Faramarzi, A., Huang, H., Zhang, D., 2021. Multi-objective optimisation design for composite tunnel linings using non-dominated sorting genetic algorithm. Geotechnical Aspects of Underground Construction in Soft Ground. CRC Press, pp. 444–450.

Zhai, W., Sun, K., Zhang, D., Huang, H., Chapman, D., 2022. An analytical solution for steel plate strengthened circular tunnels with various interface slip modes. Buildings 12 (8), 1172.

Zhang, J., Liu, X., Ren, T., Yuan, Y., Mang, H., 2019c. Structural behavior of reinforced concrete segments of tunnel linings strengthened by a steel-concrete composite. Compos. B Eng. 178 107444.

Zhang, D., Zhai, W., Huang, H., Chapman, D., 2019a. Robust retrofitting design for rehabilitation of segmental tunnel linings: Using the example of steel plates. Tunn. Undergr. Space Technol. 83, 231–242.

Zhang, D., Zhang, D., Soga, K., Huang, H., Wang, F., 2019b. Rehabilitation of overdeformed metro tunnel in shanghai by multiple repair measures. J. Geotech. Geoenviron. Eng. 145, 04019101.

Zhao, H., Liu, X., Bao, Y., Yuan, Y., Bai, Y., 2016. Simplified nonlinear simulation of shield tunnel lining reinforced by epoxy bonded steel plates. Tunn. Undergr. Space Technol. 51, 362–371.

Zidani, M.H.B., Belakhdar, K., Tounsi, A., Adda Bedia, E.A., 2015. Finite element analysis of initially damaged beams repaired with FRP plates. Compos. Struct. 134, 429–439.

Ziraba, Y., Baluch, M., 1995. Computational model for reinforced concrete beams strengthened by epoxy bonded steel plates. Finite Elem. Anal. Des. 20, 253–271.